JOURNAL OF CHEMICAL INFORMATION AND MODELING

Article

pubs.acs.org/jcim

Experimental and Quantum Chemical Modeling Studies of the Interactions of L-Phenylalanine with Divalent Transition Metal Cations

Shilpi Mandal, Gunajyoti Das,*,† and Hassan Askari

Department of Chemistry, North Eastern Hill University, Shillong-793022, India

Supporting Information

ABSTRACT: Encoded by the UUU and UUC codons of the genetic code, L-phenylalanine (LPA) serves as an important precursor for tyrosine and various other compounds that are necessary to support life on earth. Here, we report the synthesis (both in solid and solvent phases) and characterization of the Ni^{2+}, Cu^{2+}, and Zn^{2+} complexes of LPA by several analytical, spectral, thermal, and electrochemical techniques. The results reveal that the products formed by following the two synthetic approaches are the same, and the metal ions bind to the LPA molecules in a 1:2 molar ratio (M^{+2}/LPA). Complementary geometries of the metal complexes are modeled involving the most predominant LPA conformers predicted at the MP2/6-311++G(d,p) level. The gaseous and aqueous phase interaction enthalpies and free energies; theoretical IR and UV−vis spectra; HOMO−LUMO energy gaps; dipole moments; Wiberg bond indices as well as the partial atomic charges in LPA and its metallic complexes are calculated and evaluated using B3LYP/6-311++G(d,p) as the main computational method. This study also incorporates analyses on the efficacy of the DFT-D2 level in describing dispersion contributions, performance of the BHandHLYP functional for the open-shell Cu^{2+}-LPA system, and relative metal binding affinities of the singlet versus triplet states of the Ni^{2+}-LPA complex. Metal−π interactions established via the aromatic side chain of LPA add to the thermodynamic stability of the complexes, whereas metal coordination induces considerable intrinsic structural rearrangements in the molecular geometry of LPA. The LPA binding affinity order of the three Lewis acids investigated emerges as Cu^{2+} > Ni^{2+} > Zn^{2+}, paralleling the Irving−Williams series. The illustrative evidence offered by the present work suggests that the B3LYP/6-311++G(d,p) level in combination with an empirical dispersion-correction term performs well in describing the vibrational frequencies and cation−π interactions, which are undoubtedly of immense significance for natural sciences.

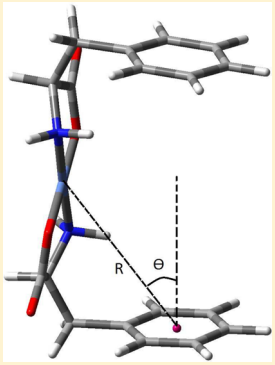

INTRODUCTION

Attraction toward metal−amino acid interactions is a corollary of the unique physical and chemical features of metalated amino acids, which bestow them with wide-ranging biological properties/activities and intriguing applicability in both application-oriented and basic scientific endeavors.[1−3] Studies on metal chelates of amino acids are at the forefront to help broaden the horizon of knowledge in the fields of prebiotic chemistry,[4] proteomics,[5] and bioorganometallics[6] and have opened promising new perspectives for scientific and industrial research.[7−10] Complexes of Ni^{2+}, Cu^{2+}, and Zn^{2+} ions with biogenic ligands are of special interest,[1,11,12] as these essential transition metal ions are engaged in a number of life processes.[13,14] Information fetched from such systems may play consequential roles in elucidating/resolving the subtleties involved in various intricate yet important biochemical processes.[1,11] Computational studies have played an immensely important role toward developments in the realm of metal−protein chemistry;[11] the complementarity of the results produced by experimental and carefully planned computational investigations has been underlined by Wormald et al.[15]

Interactions of metal ions with aromatic amino acids have received considerable attention since their aromatic side chains, in addition to the polar groups, may also interact with metal cations via noncovalent cation−π interactions:[16,17] a major force that promotes secondary structure of proteins and a host of drug−receptor interactions.[18−20] Encoded by the UUU and UUC codons of the genetic code, L-phenylalanine (LPA) is classified as a nonpolar (hydrophobic) amino acid based on the tendency of its benzyl side chain to be or not to be in contact with the aqueous environment. The biological significance of LPA has been well illustrated.[21] Several experimental and theoretical investigations have been carried out to gain insights into the complexation behavior of LPA with various metal ions.[16,17,20−26] These studies are, however, mainly focused on the gas and aqueous phase interactions of LPA with various metal ions in a 1:1 (LPA/Metal) molar ratio, except for the deprotonated dimer complex $[Zn+Phe_2-H]^+$ in the gas phase.[24] Thus, perusal of the literature highlights the need to undertake a joint experimental and computational study of the 1:2 (M^{+2}/LPA) complexes of LPA with Ni^{2+}, Cu^{2+}, and Zn^{2+} ions in vacuum, aqueous, and solid phases, to further the understanding of the metalation of LPA by transition elements. Efforts have been made in this piece of research to examine (i) the solid versus aqueous phase binding modes of LPA to metal

Received: August 15, 2014

   dx.doi.org/10.1021/ci500500k | J. Chem. Inf. Model. XXXX, XXX, XXX−XXX

ions, (ii) influence of varying d-orbital occupations of the Ni^{2+}, Cu^{2+}, and Zn^{2+} ions on structural and molecular properties of the metal−LPA complexes, (iii) effectiveness of the dispersion-corrected B3LYP methodology in describing the weak-interaction contributions to the thermodynamic stability of metalated LPA, (iv) the usefulness of B3LYP, BHandHLYP, and DFT-D2 methodologies in reproducing the experimental vibrational modes of bioactive molecules, and (v) to have a comprehensive knowledge as to how the conformational aspects of LPA may play an important part in facilitating to establish metal−π interactions via the aromatic side-chain moiety of LPA and provide additional stability to its metal complexes. It is expected that evaluation of the metal-coordinating motifs of LPA in both aqueous and solid phases as well as examination of the efficiency of B3LYP, BHandHLYP, and dispersion-corrected B3LYP levels in describing the weak interactions and vibrational frequencies of metalated LPA are valuable from the methodological point of view, which the literature is lacking up until now. The findings may also aid the pursuit of developing precise molecular mechanical force field parameters/libraries for biomacromolecular systems[27] and in promoting green chemistry.[28]

Reported herein are the synthesis and characterization of the Ni^{2+}, Cu^{2+}, and Zn^{2+} complexes of LPA in both aqueous and solid phases using conventional solvent-based and solventless mechanochemical (hand-grinding)[29,30] techniques, respectively. Solvent-free solid-state synthesis, which endows an environmentally friendly approach,[28] has often been used to obtain the targeted reaction products, a feat that the conventional solvent-phase procedures usually fail to deliver.[29] Portrayals in Figure 1

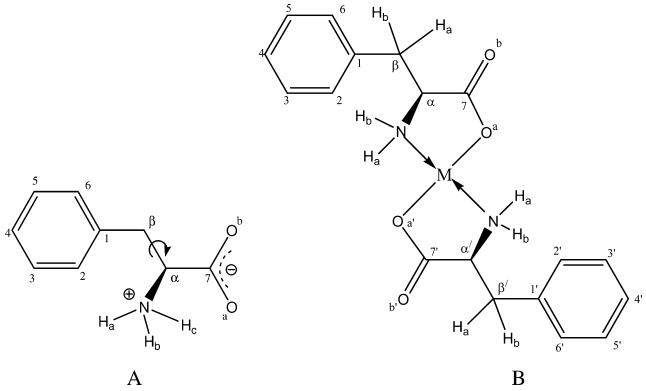

Figure 1. Portrayals displaying the molecular geometries of L-phnenylalanine (A) and its metallic complexes (B) (M = Ni^{2+}, Cu^{2+}, and Zn^{2+}); $\lambda = C_7-C_\alpha-C_\beta-C_1$.

illustrate the molecular geometries of the zwitterion LPA along with its metal complexes. The conformational aspects of the LPA molecule about the dihedral angle λ (represented by $C_7-C_\alpha-C_\beta-C_1$ in Figure 1) have been explored to be able to identify and design the metal complexes involving the most predominant conformers of LPA in the gaseous and aqueous phases. Employing various density functional based quantum chemical methodologies, theoretical calculations are conducted in a vacuum and aqueous phase to predict and analyze the thermodynamic stabilities in terms of interaction enthalpies (ΔH) and Gibbs energies (ΔG), vibrational and electronic absorption spectral properties, partial atomic charges, Wiberg bond indices, and influence of metalation on the structural aspects of LPA, together with a number of physicochemical properties of LPA and its metallic complexes. The calculations are performed considering the LPA conformers as zwitterions in the aqueous phase while as nonionic species in the gas phase.

EXPERIMENTAL TECHNIQUES

Physicochemical Measurements. IR spectra were measured from KBr discs on a BOMEM DA-8 FT-IR Spectrophotometer, while the UV/vis spectra in DMSO solution (10^{-3} M; dehydration level = 99%) were run on a PerkinElmer lambda 25 UV/vis spectrometer. Employing a coronation digital conductivity meter (cell constant = 1.0 cm^{-1}), conductivity measurements were carried out in DMSO (10^{-3} M) solution. The thermogravimetric (TG) and differential thermal analyses (DTA) were performed in a nitrogen atmosphere on a PerkinElmer STA 6000 Simultaneous Thermal Analyzer. A PerkinElmer 2400 Series II CHN-OS Analyzer was used for elemental analysis (H, C, and N). The melting points, determined on an Ikon Instrument, were not corrected. A Jeol, JSM-6360 LV apparatus was employed to acquire the EDAX-SEM images. The cyclic voltammetric measurements were also executed for the mechanochemically obtained $Cu(LPA)_2$ complex in DMSO (10^{-3} M) by means of a CH Electrochemical Analyzer. The electrolytic cell was composed of three electrodes, a glassy-carbon disc as the working, Pt-wire as auxiliary, and SCE as reference electrodes. The supporting electrolyte was 0.1 M TBAP.

Preparative Methods. AR grade L-phenylalanine (Hi Media); metal acetates of nickel, copper, and zinc; as well as the other common laboratory chemicals purchased from various sources (already mentioned in our earlier studies[29,30]) were used as received.

Solvent Free Synthesis via Mechanochemistry. In the solid the phase, LPA was made to react with the dications of nickel, copper, and zinc by following the solid-state synthetic method already described in the previous inevstigations.[29,30] After having converted the hydrated forms of the metal acetates to their anhydrous forms by drying at 108 ± 2 °C, the ligand and the dehydrated metal salts were mixed in a 1:2 molar ratio (metal/ligand) and ground at room temperature for 60 min in a grinder. To ensure complete reaction, the mixtures were kept at 90 °C in an air thermostat for 12 h and stored in sample bottles 36 h. Absolute ethyl alcohol was used to wash the final products, which were then dried under reduced pressure over anhydrous $CaCl_2$ in a desiccator. The progress of the reactions and purity of the products were monitored by TLC using silica gel G (yield: 84−91%).

Solvent-Phase Method. In the solvent phase, the metal complexes were prepared by mixing the aqueous solutions of the metal salts (50 mL, 0.1 M) with the aqueous solution of LPA (50 mL, 0.2 M) in 1:2 ratio (metal/ligand) with constant stirring. The mixtures were then heated in a water bath for 30 min. The colored precipitation formed was then cooled, filtered, and washed with water followed by absolute ethyl alcohol and placed under reduced pressure over anhydrous $CaCl_2$ in a desiccators. The reaction products were further dried in an electric oven at 60−80 °C (yield: 62−73%).

THEORETICAL BACKGROUND

To explore the rotational aspects of the LPA molecule about the dihedral angle λ ($C_7-C_\alpha-C_\beta-C_1$), the nonionic LPA molecule was initially optimized in the aqueous phase using a polarizable continuum model (PCM)[31] at the B3LYP/6-31+

dx.doi.org/10.1021/ci500500k | J. Chem. Inf. Model. XXXX, XXX, XXX−XXX

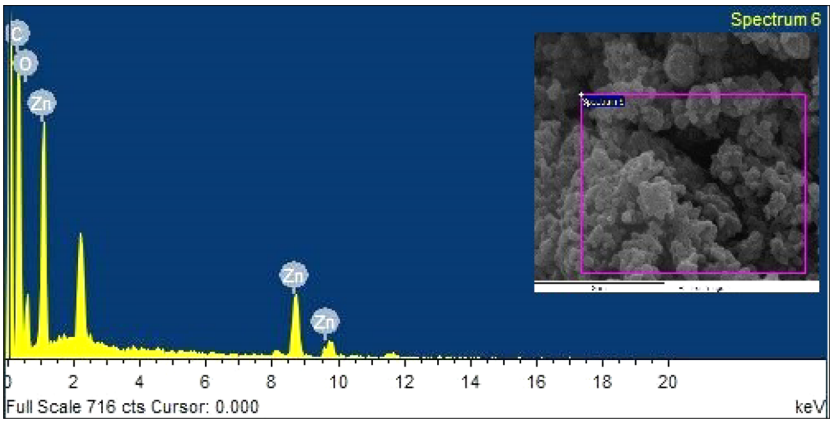

Figure 2. EDAX-SEM image for the $Zn(LPA^{C})_2$ complex prepared via mechanochemical technique (pink border is the selected area in the electron image). Visible peaks confirm the presence of carbon and oxygen substances in the sample.

+G(d,p) level of theory.[32−35] A relaxed potential energy surface (PES) scan was then performed at the same level in the aqueous phase by rotating the torsional angle λ from 0° to 360° at 20° intervals. The minima detected on the conformational PES corresponding to λ were fully optimized along with frequency calculations in gas and aqueous phases using MP2 and B3LYP methods in combination with the all-electron 6-311++G(d,p) basis set. The most stable LPA conformers predicted by the MP2 and B3LYP levels were then used to model the molecular geometries of the metal complexes of LPA with the dications of nickel, copper, and zinc. Employing the B3LYP/6-311++G(d,p) level, complete geometry optimization and subsequent frequency analyses were performed for all the gaseous and solvated reaction species involved in eqs 1 and 2. For the open-shell Cu^{2+} complexes of LPA^{B} and LPA^{C}, calculations were carried out using a spin-unrestricted formalism. Use of the BHandHLYP functional[36] was also being made for the solvated $Cu(LPA^{C})_2$ complex, since this functional is known to provide better results for open-shell systems compared to the B3LYP method.[21] Due to the possibility of the low- and high-spin states of the Ni^{2+} ion in its complexes, both the singlet and triplet states of LPA complexes of Ni^{2+} were subjected to theoretical analysis. All the computations were carried out using the Gaussian 09 (Rev. C.01) software package.[37] The optimized geometries of all the reaction species were confirmed to be true minima by the absence of any imaginary frequency value in the frequency calculations. The total energies of the reaction species were corrected for zero point vibrational energy (ZPVE) using the empirical factor 0.9877.[38,39] The vibrational frequencies below 1800 cm^{-1} were scaled with 1.01, and for those above 1800 cm^{-1} a correction factor of 0.9679 was used.[38,39] Previous studies have shown that the hybrid B3LYP model performs well in describing the interactions of the aromatic amino acids with various metal cations.[17,21,25] However, owing to its inherent architecture, the B3LYP functional of the density functional theory suffers from the inability to describe dispersion effects. Hence, we considered Grimme's dispersion corrections[40] at the DFT-D2 level as implemented in the Gaussian 09 program (Rev. C.01). The standard split-valence triple-ζ basis set in conjunction with a set of polarization and diffuse functions for both heavy and H atoms is preferred in this study, since 6-311++G(d,p) has been shown to yield qualitative accurate results in describing the interactions of various metal cations, including Ni^{2+}, Cu^{2+}, and Zn^{2+}, with biologically important chemical species.[41,42] Furthermore, adequacy of 6-311++G(d,p) in describing the molecular and electronic structural features of the divalent transition metal complexes has also been well exemplified.[43] Efficiency of the self-consistent reaction field (SCRF) model[44] as well as the usefulness of diffuse and polarization functions[45,46] have been well discussed in the literature. The interaction energies, ΔH and ΔG, were obtained from the equations given below:

$$2[H_3N^{+}CH(CH_2C_6H_5)CO_2^{-}] + M(CH_3CO_2)_2 \xrightarrow[\text{phase}]{\text{solvent}} M[H_2NCH(CH_2C_6H_5)CO_2]_2 + 2CH_3CO_2H... \quad (1)$$

$$2[H_2NCH(CH_2C_6H_5)CO_2H] + M(CH_3CO_2)_2 \xrightarrow[\text{phase}]{\text{gaseous}} M[H_2NCH(CH_2C_6H_5)CO_2]_2 + 2CH_3CO_2H... \quad (2)$$

Therefore,

$$\Delta H \text{ or } \Delta G = [P_{Et}] - [R_{Et}]$$

where M represents any of the three metal ions considered in this study and P_{Et} and R_{Et} are the sum of the ZPE corrected electronic or free energies of the products and starting materials, respectively. Time dependent density functional theory (TD-DFT)[47] single-point calculations were performed in a vacuum and DMSO at B3LYP/6-311++G(d,p) using the previously optimized geometries of LPA and its complexes to predict the theoretical λ_{max} values. Natural bond orbital (NBO) analyses were carried out using the NBO program of the Gaussian 09 suite. Structural visualizations were done by means of GaussView 5.0.8 and Chimera 1.8 molecular graphics program (http://www.cgl.ucsf.edu/chimera/).

RESULTS AND DISCUSSION

The physical, molar conductivity, and analytical data of reaction products resulted from the solid and aqueous phase interactions of LPA with the metal acetates are assembled in Table S1 of the Supporting Information (SI). The molar conductance values are suggestive of the fact that the metal−LPA compounds are neutral and nonelectrolytes.[48] The results of analyses (H, C, and N) and the proposed formula of the prepared compounds show satisfactory correspondence with the expected stoichiometries, indicating that LPA forms 1:2 (M^{+2}/LPA) complexes

dx.doi.org/10.1021/ci500500k | J. Chem. Inf. Model. XXXX, XXX, XXX−XXX

in both aqueous and solid phases. Portrayed in Figure 2 are the EDAX-SEM micrographs for the $Zn(LPA)_2$ complex synthesized in the solid phase, whereas Figure S1 displays the same for the $Zn(LPA)_2$ complex obtained in the aqueous phase as well as for the Ni^{2+} and Cu^{2+} complexes prepared in both the phases. The images bear useful insights regarding the presence of nickel, copper, and zinc in the metal−LPA complexes, their purity and particle size as well as compositional and morphological aspects. The agglomerated and homogeneous matrices of the synthesized complexes observed in the SEM micrographs indicate that the systems contain atoms in well-defined patterns and that the reactants have reacted completely to form clear homogeneous compounds. The electrochemical studies carried out on the $Cu(LPA)_2$ complex prepared by the solid-phase procedure, the cyclic voltammogram of the $Cu(LPA)_2$ complex has been depicted in Figure S2, suggest a +2 oxidation state for the copper ion in the $Cu(LPA)_2$ complex. Table S2 and Figure S3 represent the summary of the thermal measurements and TG/DTA curves respectively for the metallic LPA complexes prepared in both the phases. The TG thermograms reveal the absence of any coordinated aqua-molecule in the complexes[30] (no weight loss around 160−180 °C) and that the complexes are thermally stable up to about 239−292 °C. Beyond 239 °C, i.e. in the range of 239−684 °C, the complexes gradually decompose losing their organic components and form the corresponding metallic oxides. Completions of the reactions are indicated by the flattened TG curves beyond the T_{OF} marks. Resembling the TG thermograms, the DTA of the prepared compounds exhibit small endotherms (T_{PEAK} ∼ 254−314 °C) due to melting and broad exotherms (T_{RANGE} ∼ 400−700 °C) most probably because of decomposition to form the oxides.

Modeling the Complexes of LPA. From the earlier experimental and theoretical studies,[16,24,25] it is clear that the conformational aspects of the LPA molecule about the dihedral angle λ (Figure 1) play a crucial role in determining the energetics and existence of cation−π interactions in its metal complexes. Therefore, a conformational analysis was performed on the nonionic LPA molecule about its λ dihedral angle to determine the most stable gas-phase nonionic and aqueous-phase zwitterionic LPA conformers. Figure 3 depicts the potential energy surface plot corresponding to the dihedral angle λ while Figure 4 depicts the MP2/6-311++G(d,p) level optimized geometries of the three LPA conformers viz. LPA^A (λ ∼ 70°), LPA^B (λ ∼ 170°), and LPA^C (λ ∼ −70°) in their nonionic and zwitterionic forms. The relative energies, ZPVE values, total electronic (E), and Gibbs energies (G) as well as the ZPVE corrected values of E and G (E_C and G_C respectively) for all the three conformers are listed in Table S1. These data suggest that the two most stable conformers LPA^B and LPA^C corresponding to the dihedral angle λ do not differ significantly from each other in terms of their relative thermodynamic stability and fall within a narrow energy range of 0.06 to 0.85 kcal/mol in both the phases. Thus, we modeled the metal complexes of LPA with the dications of nickel, copper, and zinc using the conformers LPA^B and LPA^C. The aqueous phase DFT(B3LYP) optimized geometries of the metal complexes arising from LPA^B and LPA^C are depicted in Figure 5 while their gaseous and aqueous phase ZPVE, E, G, E_C, and G_C values calculated using B3LYP, BHandHLYP, and dispersion-corrected B3LYP (at DFT-D2) methods in combination with the 6-311++G(d,p) basis set are summarized in Table S4.

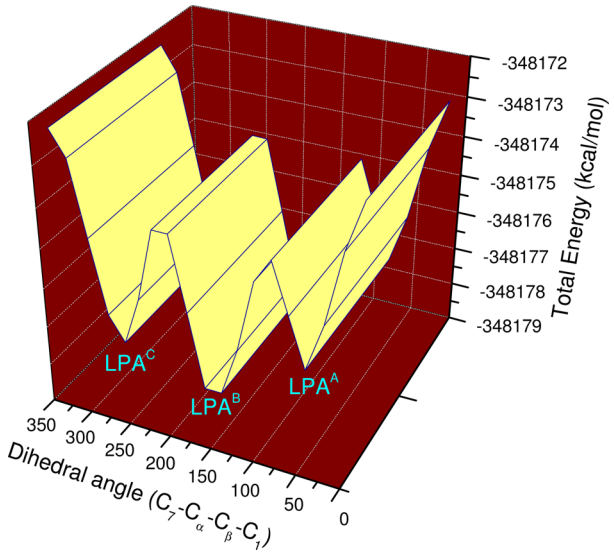

Figure 3. 3D plot of total electronic energy (ZPE-uncorrected) versus torsional angle λ (C_7−C_α−C_β−C_1) for rotation about the C_α−C_β bond (starting from 0° to 360° at 20° intervals) of the nonionic LPA molecule at the B3LYP/6-31++G(d,p) level in the aqueous phase.

Geometry, Stability, and Electronic Properties. As evident from Figure 5, the Ni^{2+} and Cu^{2+} complexes of LPA^B and LPA^C show square-planar types of geometries, while the Zn^{2+} complexes adopt nearly tetrahedral geometries in both the phases. The predicted geometries of the complexes are in good agreement with the results of previous studies.[24,30,49] On the other hand, it is well-known that cation−π interactions established by the aromatic rings of various biomolecules are purely electrostatic in nature that can operate over a large distance (up to nearly 5.0 Å) under physiological conditions.[50,51] Assessment of such weak noncovalent interactions by the common experimental techniques is difficult.[52,53] Computational studies on the geometry of the cation−π interactions have confirmed that the cation must interact with the face of the ring. Electronic properties like polarizability and aromaticity of the rings are not the defining features for such interactions.[50] From the MP2 and B3LYP level predicted geometries of LPA^B, LPA^C, and their metal complexes, depicted in Figures 4 and 5, respectively, it is clear that the metal−aromatic π interactions are not possible in the complexes of LPA^B since the amino group of this conformer is positioned right in between the metal cation and π-electron cloud of the aromatic ring. In contrast, analysis of the geometrical conditions[51] (displayed in Figure 6 for the $Ni(LPA^C)_2$ complex) reveals that metal−π interactions are possible in the case of the complexes arising from the conformer LPA^C. The R and θ values for the three metal−LPA^C complexes are listed in Table S5. Assembled in Table 1 are the gaseous and aqueous phase data on ΔH, ΔG, HOMO−LUMO energy gaps (E_{HL}), and dipole moments (μ) of LPA^B and LPA^C as well as their metal complexes, obtained by employing different DFT based quantum chemical methodologies. As predicted at the B3LYP/6-311++G(d,p) level, the interaction enthalpies (−24.79 to −67.43 kcal/mol in aqueous phase and −41.16 to −80.45 kcal/mol in vacuum) and free energies (−24.16 to −65.16 kcal/mol in aqueous phase and −38.20 to −75.08 kcal/mol in vacuum) for all the systems suggest that the metal−LPA complexes are thermodynamically stable. In view of the B3LYP level data on the energies of the complexes, the cation-binding affinity order of LPA appears to

dx.doi.org/10.1021/ci500500k | J. Chem. Inf. Model. XXXX, XXX, XXX−XXX

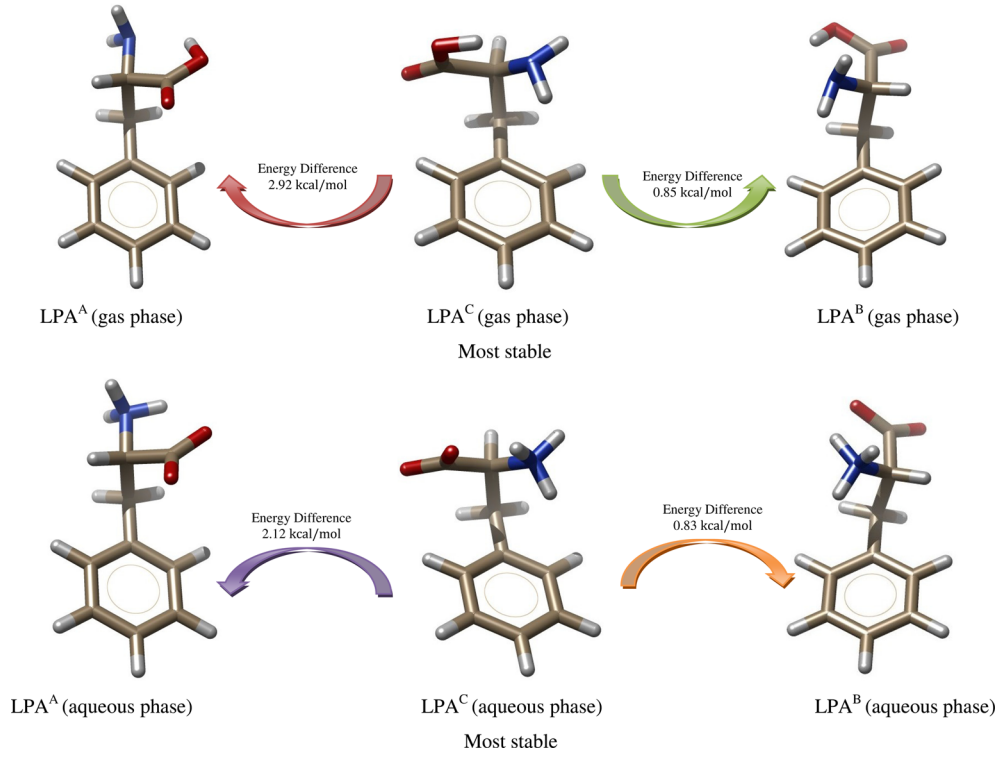

Figure 4. Three possible conformers of LPA corresponding to λ (C_7–C_α–C_β–C_1) at the MP2 level.

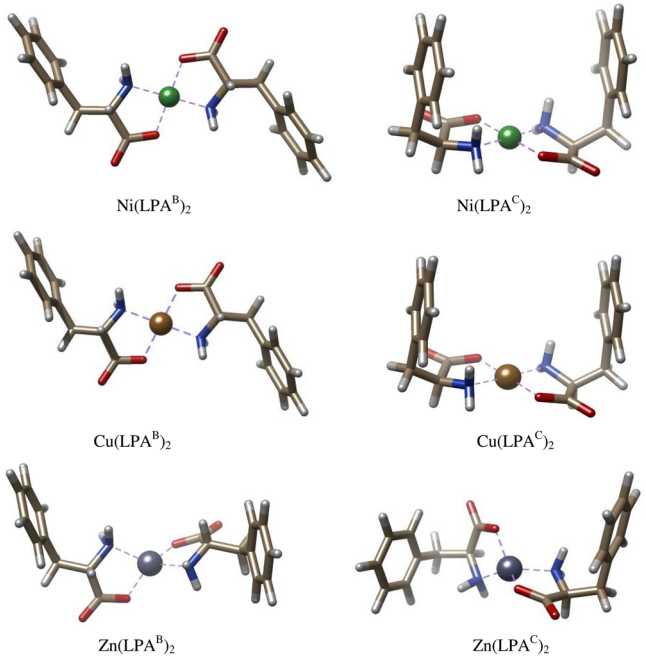

Figure 5. Optimized geometries of the solvated metallic complexes arising from LPA^B and LPA^C.

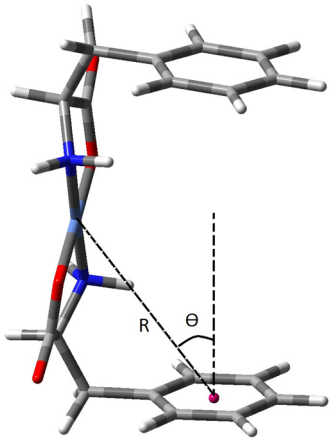

Figure 6. Depiction of the geometrical conditions describing metal–π interactions in the $Ni(LPA^C)_2$ complex optimized at B3LYP/6-311++G(d,p).

be Ni^{2+} > Cu^{2+} > Zn^{2+} in both the phases. However, the BHandHLYP functional, capable of effectively describing the spin-delocalized situations in an open-shell system like the $Cu(LPA^C)_2$ complex, outperforms the B3LYP method and predicts an interaction enthalpy of −72.07 kcal/mol (ΔG = −69.41 kcal/mol) in the aqueous phase.[25] This suggests the Cu^{2+} ion to be the strongest Lewis acid (possesses highest affinity to LPA) giving a binding affinity order of Cu^{2+} > Ni^{2+} > Zn^{2+} across the series of metal ions investigated in the current study, which is in precise agreement with the Irving–Williams series. Regarding the stability of the high- and low-spin states of the Ni^{2+}–LPA complexes, the B3LYP level thermodynamic data presented in Table 1 (for example, aqueous phase ΔH values of the $^e Ni(LPA^B)_2$ and $^e Ni(LPA^C)_2$ complexes in their triplet states are −22.30 and −18.59 kcal/mol while those of $Ni(LPA^B)_2$ and $Ni(LPA^C)_2$ are −67.35 and −67.43 kcal/mol) clearly show that the square planar Ni^{2+} complexes of LPA^B and LPA^C exist in their singlet forms. Hence, the physicochemical properties of the $^e Ni(LPA^B)_2$ and $^e Ni(LPA^C)_2$ complexes are not discussed further. On the other hand, it is interesting to note that the DFT(B3LYP) level predicts all the metal complexes of the LPA^C conformer to be somewhat more stable compared to those arising from LPA^B in both the two phases, even though the same level predicts LPA^B to be more

dx.doi.org/10.1021/ci500500k | J. Chem. Inf. Model. XXXX, XXX, XXX–XXX

Table 1. Summary of Thermodynamic (Cation-Binding Enthalpies ΔH and Free Energies[a] ΔG) and Electronic (HOMO−LUMO Energy Gaps[b] E_{HL} and Dipole Moments[c] μ) Properties of LPA Conformers and Their Complexes Calculated at B3LYP/6-311++G(d,p) Level

compounds	ΔH	ΔG	ΔH^d	ΔG^d	E_{HL}	μ
LPA^B					6.126 (5.915)	13.25 (2.56)
LPA^C					6.205 (6.194)	12.85 (5.18)
$Ni(LPA^B)_2$	−67.35 (−79.56)	−65.10 (−75.02)	−75.27 (−78.82)	−66.25 (−70.43)	4.784 (4.769)	0.10 (0.35)
$Ni(LPA^B)_2$[e]	−22.30 (−13.16)	−20.15 (−10.83)				
$Ni(LPA^C)_2$	−67.43 (−80.45)	−65.16 (−75.08)	−76.41 (−80.91)	−66.89 (−70.90)	4.774 (4.677)	0.41 (0.85)
$Ni(LPA^C)_2$[e]	−18.59 (−14.57)	−16.93 (−11.42)				
$Cu(LPA^B)_2$	−53.84 (−43.36)	−49.06 (−39.71)	−55.98 (−47.44)	−39.02 (−38.19)	6.006 (5.602)	0.15 (0.43)
$Cu(LPA^C)_2$	−53.90 (−44.51)	−49.53 (−39.99)	−57.36 (−49.81)	−40.98 (−40.31)	5.958 (5.575)	0.79 (1.25)
$Cu(LPA^C)_2$[f]	−72.07	−69.41				0.70
$Zn(LPA^B)_2$	−24.79 (−41.16)	−24.16 (−38.20)	−26.77 (−43.22)	−24.32 (−37.10)	6.163 (5.583)	11.94 (8.24)
$Zn(LPA^C)_2$	−25.04 (−41.33)	−24.53 (−38.52)	−27.40 (−44.60)	−22.64 (−40.00)	6.241 (5.498)	11.72 (6.68)

[a]Energies in kcal/mol. [b]E_{HL} in eV. [c]μ in Debye. [d]Dispersion-corrected values at DFT-D2 level. [e]Triplet. [f]Calculated using BHandHLYP/6-311++G(d,p) method. The aqueous phase interaction energies are calculated using the ZPVE corrected total electronic and free energies of the zwitterionic structures of the LPA conformers. Values in parentheses are from gas phase calculations.

stable compared to LPA^C (see Table S3). We attribute the extra stability exhibited by the metallic complexes of LPA^C at the B3LYP level to metal−π interactions, established by the aromatic π-electron cloud of the side-chain moiety of the LPA^C conformer with the Ni^{2+}, Cu^{2+}, and Zn^{2+} ions. In order to study the influence of metal−π interactions on the thermodynamic parameters of the complexes in more detail, we ventured to perform additional dispersion-corrected DFT calculations at the DFT-D2 level for all the metal complexes arising from LPA^B and LPA^C conformers. The gas and aqueous phase dispersion-corrected values of the interaction enthalpies (ΔH^d) and Gibbs energies (ΔG^d) of the complexes are gathered in Table 1 (the geometrical parameters after dispersion-correction are listed in Table S5). It is evident from these data that the energy separations between the complexes of LPA^C and LPA^B are increased after including an empirical dispersion-correction term in the calculations. For example, difference between the ΔH^d values of the $Cu(LPA^C)_2$ and $Cu(LPA^B)_2$ complexes is predicted to increase up to 2.37 kcal/mol in the gaseous phase and 1.38 kcal/mol in the aqueous phase. This, together with the similar situations observed in the cases of Ni^{2+} and Zn^{2+} complexes, suggests that the B3LYP/6-311++G(d,p) level in conjunction with an empirical dispersion-correction term performs well in describing the metal-aromatic π-interaction contributions to the thermodynamic stability of the biologically relevant chemical species. Since there is evidence that aromatic amino acids are capable of establishing cation−π interactions in all three phases viz. solid, liquid, and gas, it is reasonable to assume that it is the predominant LPA^C conformer which formed the metal complexes with Ni^{2+}, Cu^{2+}, and Zn^{2+} ions in our solid and liquid phase experiments.

The gas and aqueous phase Mulliken, natural population analysis (NPA), and Merz−Kollman electrostatic potential (ESP) charges for LPA^C and its complexes calculated using the B3LYP and BHandHLYP methods in combination with the 6-311++G(d,p) basis set are summarized in Table S6. Displayed in Figure S4 are the molecular electrostatic potential (MEP) charge distributions for LPA^C and its complexes in the solution phase, where the electrophilic and nucleophilic centers are symbolized by red and blue colorations, respectively. These depictions provide a visual description about the studied systems concerning the possible reactivity of different atomic sites toward electrophilic and nucleophilic reagents, besides their spectroscopic features. The furnished NPA charges offer useful insights about the effects of different d-orbital occupations of the Ni^{2+}, Cu^{2+}, and Zn^{2+} ions on the charge distribution of the LPA^C molecule due to metalation. It is apparent from Table S6 that the atomic charges upon N, O_a, O_b, C_7, and C_α atoms of LPA^C are altered significantly based on the individuality of the metalating cation. It is interesting to note here that Cu^{2+} ion markedly decreases the charge densities on the NH_2 and COO^- functions of LPA^C than Ni^{2+} and Zn^{2+} ions, presenting itself as the strongest Lewis acid out of the three metal cations. Thus, the data on the partial atomic charges support the metal-binding affinity order, i.e. Cu^{2+} > Ni^{2+} > Zn^{2+}, predicted on the basis of the thermodynamic parameters, ΔH and ΔG.

The energy gaps (E_{HL}) between the highest occupied molecular orbital (HOMO) and lowest unoccupied molecular orbital (LUMO) energies for the gaseous and solvated systems are presented in Table 1, whereas the aqueous phase HOMO and LUMO plots of the LPA^C conformer and its complexes are depicted in Figure S5. The data produced herein indicate that the E_{HL} values of the reaction species (4.677−6.194 eV in vacuum and 4.774−6.241 eV in solvated states) increase due to the solvation effects of the aqueous environment. These results are consistent with the previous theoretical observations and serve as the indication of increased stability of the reaction species in the aqueous phase.[39] The predicted total dipole moments of LPA^B, LPA^C, and their metal complexes at the B3LYP and BHandHLYP levels are collected in Table 1. The tetrahedral Zn^{2+} complexes exhibit much larger μ values (up to 11.94 D in the aqueous phase and 8.24 D in the gas phase) than the square-planar Ni^{2+} and Cu^{2+} complexes (0.10 to 0.79 D for the solvated systems and 0.35 to 1.25 D in vacuum). Greater μ values of the Zn^{2+} complexes are indicative of their higher polar character and stronger affinity for polar solvents. These large μ values may aid future gas-phase studies of these complexes involving microwave spectrum and permanent electric dipole analyses. The 1:2 complex of LPA with the Zn^{2+} ion might also serve as a better nonlinear optical material compared to the Ni^{2+} and Cu^{2+} complexes since high μ values often suggest better NLO properties of a compound. Furthermore, both the B3LYP and BHandHLYP functional yield comparable μ values for the solvated $Cu(LPA^C)_2$ complex.

dx.doi.org/10.1021/ci500500k | J. Chem. Inf. Model. XXXX, XXX, XXX−XXX

Table 2. Observed and B3LYP/6-311++G(d,p) Level Predicted IR Assignments for LPA and Its Metal Complexes[a]

			vibrational modes (cm^{-1})											
systems	methods		ν_{as}(N−H)	ν_{s}(N−H)	ν(O_a−H)	ν_{aro}(C−H)	ν(C_α−H)	ν_{as} (COO^-)	ν_{s}(COO^-)	ν(C_α−N)	ν(C_7−O_a)	ν(M−O)	ν(M−N)	$\Delta\gamma$
LPA	expt.	I	3312	3164		3066	2886	1556	1413	1163	1225			143
	theo	III	3414 (3469)	3359 (3393)	-- (3415)	3059 (3058)	3033 (2944)	1683 (1781)	1442 (1412)	1113 (1084)	1325 (1231)			241 (369)
		IV	3410 (3462)	3345 (3395)	-- (3479)	3058 (3053)	3023 (2934)	1684 (1776)	1441 (1431)	1149 (1116)	1305 (1221)			243 (345)
		V	3410 (3476)	3321 (3385)	-- (3346)	3065 (3064)	2998 (2930)	1680 (1768)	1435 (1426)	1111 (1121)	1223 (1249)			245 (342)
$Ni(LPA)_2$	expt.	I	3358	3301		3029	2926	1634	1404	1102	1259	554b	465s	230
		II	3357	3306		3029	2939	1626	1404	1101	1258	551b	467s	222
	theo.	IV	3428 (3420)	3356 (3355)		3067 (3052)	2967 (2956)	1687 (1773)	1352 (1348)	1080 (1073)	1326 (1306)	522 (533)	492 (494)	335 (425)
		V	3422 (3413)	3322 (3324)		3064 (3063)	2963 (2959)	1685 (1768)	1350 (1331)	1109 (1120)	1291 (1280)	530 (561)	441 (449)	335 (437)
		VI	3416 (3409)	3319 (3311)		3064 (3063)	2977 (2963)	1680 (1761)	1356 (1332)	1077 (1070)	1291 (1280)	573 (541)	442 (451)	338 (429)
$Cu(LPA)_2$	expt.	I	3333	3250		3032	2943	1618	1395	1105	1234	557s	468s	223
		II	3333	3250		3032	2942	1612	1394	1105	1234	557s	468s	218
	theo	IV	3438 (3433)	3368 (3366)		3057 (3051)	2965 (2954)	1683 (1761)	1352 (1347)	1080 (1071)	1331 (1309)	550 (544)	409 (420)	331 (414)
		V	3433 (3427)	3343 (3336)		3064 (3063)	2958 (2953)	1675 (1758)	1350 (1328)	1101 (1111)	1292 (1284)	542 (543)	423 (423)	325 (430)
		VI	3425 (3417)	3314 (3306)		3055 (3051)	2962 (2958)	1670 (1659)	1354 (1329)	1105 (1099)	1290 (1277)	554 (553)	459 (163)	316 (330)
		VII	3451	3374		3105	2986	1750	1479	1131	1352	614	536	271
$Zn(LPA)_2$	expt.	I	3334	3257		3029	2957	1611	1407	1087	1253	559w	471s	204
		II	3334	3257		3029	2957	1611	1407	1087	1252	558w	470s	204
	theo.	IV	3439 (3425)	3370 (3356)		3057 (3050)	2967 (2950)	1668 (1765)	1366 (1346)	1111 (1112)	1339 (1316)	585 (580)	491 (491)	302 (419)
		V	3439 (3421)	3357 (3323)		3063 (3063)	2951 (2948)	1664 (1761)	1355 (1330)	1072 (1066)	1244 (1287)	538 (536)	494 (493)	309 (431)
		VI	3439 (3431)	3346 (3316)		3063 (3064)	2964 (2956)	1664 (1754)	1373 (1330)	1075 (1063)	1241 (1285)	580 (581)	491 (492)	291 (424)

[a]I = solid state; II = solvent phase; III = LPA^A; IV = LPA^B and its complexes; V = LPA^C and its complexes; VI = dispersion-corrected values for complexes of LPA^C; VII = calculated at BHandHLYP/6-311++G(d,p) method for $Cu(LPA^C)_2$; b = broad; s = strong; w = weak. Frequency values below 1800 cm^{-1} are scaled with 1.01 and for those above 1800 cm^{-1} a correction factor 0.9679 is used. Values in parentheses are from gas phase calculations.

dx.doi.org/10.1021/ci500500k | J. Chem. Inf. Model. XXXX, XXX, XXX−XXX

Table 3. Electronic Absorption Spectral Data for the Ligand and Complexes[a]

	$\lambda_{max\ (nm)}$						
	experimental					calculated	
systems	solid state	ε	aqueous phase	ε	assignments	DMSO	gas phase
LPA	249	11027			due to intraligand n−π^* and π−π^* transition	219 (226)	242 (231)
	290	59592					
	292	140029					
	312	3576					
$Ni(LPA)_2$	275	115980	275	1757	n−π^*	637 (636)	621 (622)
	338	148721	375	1971	π−π^*		
	413	54355			LMCT		
	549	21266	550	1256	$^1A_{1g}\rightarrow{}^1B_{1g}$ transition		
$Cu(LPA)_2$	289	135152	273	390975	n−π^*	591 (633)	578 (612)
	346	112206	337	126860	π−π^*		
	379	13616	383	203678	LMCT		
			412	185650	LMCT		
	620	2187	607	1194	$^2B_{1g}\rightarrow{}^2A_{1g}$ transition		
$Zn(LPA)_2$	289	29040	210	2228	n−π^*	234 (235)	252 (259)
	335	41725	274	2177	π−π^*		
	383	58771	372	2666	LMCT		

[a]Values for LPA^B are given in parentheses; ε = molar extinction coefficient in L $mol^{-1}cm^{-1}$.

Vibrational Spectroscopy of Metalated LPA. Tabulated in Table 2 are the pertinent FT-IR assignments of LPA and its metal complexes synthesized using the conventional solvent-based and solvent-free mechanochemical grinding techniques, whereas their experimental FT-IR spectra are stored in the SI (Figure S6). The summarized data on the vibrational bands reveal the absence of any unbound/unreacted LPA molecule in the reaction products, besides illustrating the essentially similar metal-binding patterns of LPA in both the aqueous and solid phases. As evident from Table 2, the asymmetric and symmetric ν(N−H) stretching modes of LPA (observed at 3312 and 3164 cm^{-1}, respectively) are shifted to higher wave numbers in the complexes (3333−3358 and 3250−3306 cm^{-1}, respectively). These frequency shifts suggest deprotonation of the NH_3^+ group of zwitterion LPA and its subsequent binding to the metal cations via the amino N atom.[30] Involvement of the N atom in metalation is also evidenced by the emergence of asymmetric ν(M−N) bands at 465−471 cm^{-1} for the metal−LPA complexes[54] as well as the lowering of the $\nu(C_\alpha-N)$ stretching frequencies in the complexes (1087−1105 cm^{-1}) as compared to that in metal-free LPA (1163 cm^{-1}).[30] It is worth mentioning that the two coordinating $-NH_2$ groups are positioned *trans* to each other in the metal complexes since the symmetric ν(M−N) stretching mode of the N−M−N group (M = Ni^{2+}, Cu^{2+}, and Zn^{2+}) which usually appears around 400−450 cm^{-1} is IR inactive.[54] Indication of metal binding via the carboxylate group of LPA is evident from the observations that the $\nu_{as}(COO^-)$ stretch of LPA appearing at 1556 cm^{-1} shows blue shift (up to 1634 cm^{-1}) as a consequence of metal binding whereas the $\nu_s(COO^-)$ mode of LPA at 1413 cm^{-1} exhibits a red shift after metalation (1394−1407 cm^{-1}).[30] The differences ($\Delta\gamma$ values) between the $\nu_{as}(COO^-)$ and $\nu_s(COO^-)$ stretches for LPA and its complexes, listed in Table 2, present themselves as the measure of the M−O bond strengths, which further indicate the monodentate type of metal-coordinating motif of the COO^- moeity.[55] Spanning a scale of 204 to 230 cm^{-1}, the $\Delta\gamma$ values bear additional information regarding the significantly large covalent character in the M−O bonds of the complexes.[30] The peaks at 551−559 cm^{-1} in the metal complexes, assigned to ν(M−O) stretching frequencies,[30] also validate the participation of the carboxylate group of LPA in metal coordination. The bands at 3029−3066 cm^{-1} and 2886−2957 cm^{-1} can be assigned to aromatic ν_{aro}(C−H) and $\nu(C_\alpha-H)$ stretching vibrations, respectively.

The theoretical IR spectra of LPA^A, LPA^B, and LPA^C as well as the metallic complexes of LPA^B and LPA^C were computed in a vacuum and aqueous phase using the B3LYP/6-311++G(d,p) level. Table 2 assembles a set of key frequency values of the reaction species, whereas their predicted IR spectra are given in the SI (Figure S7; scaled with 0.955). The often-encountered inconsistencies between the predicted and experimentally observed frequencies owing to certain technical shortcomings of the theoretical methodologies have been discussed in the literature.[56] On the other hand, the B3LYP functional has been proven time and again to perform well in complementing the experimental vibrational data.[57−59] It is clear from the data amassed in Table 2 that the theoretically predicted vibrational modes of the LPA^C and its complexes are more close to the experimentally observed FT-IR assignments of LPA and its metal complexes compared to those of LPA^A, LPA^B, and the metallic complexes of LPA^B. Thus, the theoretical vibrational data calculated at the B3LYP/6-311++G(d,p) level reinforce the thermodynamic parameters (listed in Table 1) in supporting that the metal complexes of LPA with the Ni^{2+}, Cu^{2+}, and Zn^{2+} ions are formed by the most predominant LPA^C conformer in our solid- and liquid-phase experiments. On the other hand, $\nu(C_\alpha-H)$, $\nu(C_7-O_a)$, ν_{as}(N−H), and ν_s(N−H) modes of the complexes vary significantly from LPA which are presumably due to the changes in the geometries about the C_α, C_7, and N atom of LPA as a result of metal-binding. Furthermore, the theoretical frequency shifts of the ν_{as}(N−H), ν_s(N−H), $\nu_{as}(COO^-)$, and $\nu_s(COO^-)$ bands of LPA after metalation show fine corroboration to the experimental results. The theoretical values of ν(M−O) and ν(M−N) modes are also in good agreement with the experimentally obtained frequencies. Table 2 also incorporates the gas and aqueous phase vibrational data for the metal complexes arising from the LPA^C conformer calculated using the dispersion-corrected

dx.doi.org/10.1021/ci500500k | J. Chem. Inf. Model. XXXX, XXX, XXX−XXX

Table 4. Pertinent Bond Distances (in Ångstrom), Bond Angles, and Dihedral Angles (in Degrees) for LPA^B, LPA^C, and Their Metal Complexes Calculated at the B3LYP/6-311++G(d,p) Level in Vacuum and Aqueous Environments[a]

bond distances	LPA^B	LPA^C	$Ni(LPA^B)_2$	$Ni(LPA^C)_2$	$Cu(LPA^B)_2$	$Cu(LPA^C)_2$	$Zn(LPA^B)_2$	$Zn(LPA^C)_2$	LV^B	LV^C
C_α–C_7	1.563 (1.520)	1.568 (1.548)	1.542 (1.550)	1.542 (1.551)	1.549 (1.557)	1.548 (1.558)	1.557 (1.565)	1.556 (1.566)	0.021 (0.045)	0.026 (0.018)
C_α–C_β	1.541 (1.563)	1.538 (1.549)	1.536 (1.534)	1.542 (1.541)	1.538 (1.536)	1.544 (1.543)	1.539 (1.538)	1.547 (1.544)	0.005 (0.029)	0.009 (0.008)
C_α–N	1.512 (1.459)	1.511 (1.471)	1.491 (1.494)	1.491 (1.493)	1.488 (1.491)	1.488 (1.490)	1.489 (1.497)	1.490 (1.496)	0.024 (0.038)	0.023 (0.025)
C_β–C_1	1.516 (1.511)	1.515 (1.514)	1.515 (1.513)	1.516 (1.515)	1.515 (1.513)	1.515 (1.515)	1.539 (1.513)	1.516 (1.515)	0.023 (0.002)	0.001 (0.001)
C_7=O_b	1.249 (1.205)	1.242 (1.204)	1.226 (1.213)	1.226 (1.215)	1.228 (1.215)	1.229 (1.217)	1.232 (1.216)	1.234 (1.218)	0.023 (0.011)	0.016 (0.014)
C_7–O_a	1.268 (1.356)	1.262 (1.337)	1.300 (1.309)	1.300 (1.306)	1.295 (1.304)	1.294 (1.301)	1.288 (1.299)	1.286 (1.297)	0.032 (0.057)	0.038 (0.040)
M–O			1.866 (1.850)	1.866 (1.851)	1.945 (1.913)	1.944 (1.916);[b]1.932	2.001 (1.927)	1.998 (1.926)		
M–N			1.928 (1.923)	1.928 (1.922)	2.021 (2.032)	2.020 (2.029);[b]2.017	2.100 (2.111)	2.092 (2.114)		
[c]M–O			0.338 (0.366)	0.337 (0.362)	0.182 (0.210)	0.182 (0.207);[b]0.300	0.149 (0.179)	0.136 (0.179)		
[c]M–N			0.366 (0.356)	0.364 (0.357)	0.207 (0.187)	0.199 (0.188);[b]0.274	0.189 (0.136)	0.176 (0.134)		
bond angle	LPA^B	LPA^C	$Ni(LPA^B)_2$	$Ni(LPA^C)_2$	$Cu(LPA^B)_2$	$Cu(LPA^C)_2$	$Zn(LPA^B)_2$	$Zn(LPA^C)_2$	LV^B	LV^C
N–C_α–C_7	106.0 (110.6)	106.0 (109.5)	107.8 (108.3)	108.3 (108.1)	109.1 (109.7)	109.7 (109.6)	110.5 (111.4)	111.7 (111.4)	4.5 (2.3)	5.7 (1.9)
N–C_α–C_β	111.2 (116.1)	112.2 (115.8)	113.9 (113.5)	113.7 (113.9)	113.6 (113.4)	113.5 (113.6)	113.3 (112.9)	112.8 (113.1)	2.7 (3.2)	1.5 (2.7)
C_7–C_α–C_β	111.6 (108.1)	115.6 (111.7)	113.5 (112.9)	114.3 (113.8)	113.1 (112.5)	113.8 (113.2)	112.7 (112.1)	112.8 (112.7)	1.9 (4.8)	2.8 (2.1)
O_b-C_7–O_a	128.9 (122.6)	129.0 (123.0)	124.2 (125.4)	124.1 (125.4)	124.3 (125.5)	124.3 (125.5)	124.7 (126.0)	124.8 (125.9)	4.7 (3.4)	4.9 (2.9)
C_α–C_7–O_a	115.0 (112.2)	114.8 (113.9)	114.5 (113.9)	114.9 (114.0)	115.6 (115.0)	116.1 (115.3)	116.5 (116.2)	117.5 (116.5)	1.5 (4.0)	2.7 (2.6)
C_α–C_7–O_b	116.1 (125.2)	116.2 (123.0)	121.3 (120.6)	120.9 (120.5)	120.0 (119.4)	119.5 (119.2)	118.7 (117.7)	117.7 (117.6)	5.2 (7.5)	4.7 (5.3)
C_α–C_β–C_1	114.0 (112.4)	114.6 (114.1)	113.7 (113.6)	114.6 (114.2)	113.7 (113.6)	114.6 (114.0)	113.7 (113.4)	114.5 (113.9)	0.3 (1.2)	0.1 (0.2)
dihedrals	LPA^B	LPA^C	$Ni(LPA^B)_2$	$Ni(LPA^C)_2$	$Cu(LPA^B)_2$	$Cu(LPA^C)_2$	$Zn(LPA^B)_2$	$Zn(LPA^C)_2$	LV^B	LV^C
N–C_α–C_7–O_a	−10.2 (−42.5)	6.5 (11.9)	18.9 (17.5)	14.2 (17.7)	19.8 (18.3)	13.5 (17.2)	20.6 (16.5)	7.8 (15.2)	10.4 (26.0)	7.7 (3.3)
N–C_α–C_7–O_b	170.8 (140.6)	−175.4 (−170.3)	−163.5 (−164.7)	−168.5 (−164.9)	−162.9 (−164.1)	−169.4 (−165.5)	162.3 (−166.3)	−174.5 (−167.7)	8.5 (25.7)	6.9 (5.4)
O_a–C_7–C_α–C_β	111.0 (85.7)	131.5 (141.5)	146.1 (144.1)	142.2 (145.3)	147.3 (145.5)	141.8 (145.2)	148.5 (144.1)	136.1 (143.6)	37.5 (59.8)	10.7 (3.8)
C_α–C_β–C_1–C_6	−69.7 (−77.7)	78.1 (80.5)	−72.5 (−73.8)	81.2 (78.0)	−73.0 (−73.9)	80.6 (78.8)	−73.0 (−74.3)	80.2 (77.4)	3.3 (3.9)	3.1 (3.1)
C_α–C_β–C_1–C_2	109.5 (100.9)	−101.4 (−98.7)	107.3 (105.2)	−98.3 (−101.2)	106.7 (105.3)	−98.9 (−100.3)	106.8 (104.6)	−99.4 (−101.6)	2.8 (4.4)	3.1 (2.9)

[a] LV^B and LV^C are the largest variation from LPA^B and LPA^C. [b] Calculated using BHandHLYP/6-311++G(d,p) method. [c] Wiberg bond indices. Values in parentheses are from gas phase calculations.

dx.doi.org/10.1021/ci500500k | J. Chem. Inf. Model. XXXX, XXX, XXX−XXX

B3LYP (at DFT-D2) method in combination with a 6-311++G(d,p) basis set, alongside the aqueous phase vibrational frequencies for the $Cu(LPA^C)_2$ system calculated at the BHandHLYP/6-311++G(d,p) level. Apart from the $\nu(C_\alpha-H)$ vibrational mode, almost all the other vibrational frequency values of the metal complexes predicted by the dispersion-corrected B3LYP method give a more close fitting to the experimental spectra, suggesting that the B3LYP/6-311++G(d,p) level in combination with an empirical dispersion-correction term performs well in describing the vibrational spectroscopy of the bioactive molecules. On other hand, the harmonic frequencies of the $Cu(LPA^C)_2$ system predicted at the BHandHLYP/6-311++G(d,p) level are markedly higher as compared to the experimentally observed FT-IR assignments of the $Cu(LPA)_2$ complex as well as to those obtained by using the B3LYP/6-311++G(d,p) or the dispersion-corrected B3LYP/6-311++G(d,p) levels, indicating that B3LYP outshines the BHandHLYP functional in reproducing the experimental infrared assignments.

UV−Vis Spectroscopy. The theoretical and experimental results of the electronic absorption spectral studies are presented in Table 3, whereas Figures S8 and S9 portray the predicted and observed UV−vis spectra of the reaction species. The absorption bands associated with the UV−vis spectrum of a given transition metal complex can often be used to infer its coordination geometry. For example, it is well-known that square planar Cu(II) complexes usually give a broad absorption band between 600 and 700 nm owing to Jahn−Teller distortion. LPA and all the reaction products obtained from the grinding or solvent-based procedures display intense bands at 210−346 nm which are assigned to intraligand n → π^* and π → π^* transitions. The less intense peaks at 372−413 nm (observed only for the metallic complexes of LPA) are because of LMCT transitions confirming the formation of the complexes. Furthermore, the presence of the much weaker and less well-defined broad bands in the spectra of $Ni(LPA)_2$ (∼550 nm) and $Cu(LPA)_2$ (spanning a scale of 607−620 nm) complexes, which may be due to the $^1A_{1g}$ → $^1B_{1g}$ and $^2B_{1g}$ → $^2A_{1g}$ transitions, support the DFT predicted square planar type geometries for the Ni^{2+} and Cu^{2+} complexes of LPA.[60] These d−d transitions are absent in the UV−vis spectrum of the Zn^{2+} complex because of the fully filled d orbital of the Zn^{2+} ion.[61] The calculated UV−vis spectra of LPA and its complexes determined in a vacuum and DMSO using TD-DFT at the B3LYP/6-311++G(d,p) level, known for its efficacy to accurately describe the λ_{max} values,[29,30] exhibit characteristic λ_{max} values in the range 219−637 nm. The experimentally observed d−d transitions at ∼549−620 nm, which appear only in the UV−vis spectra of Ni^{2+} and Cu^{2+} complexes of LPA, are well complemented in the TD-DFT studies (λ_{max} ∼ 591−637 nm).

Structural Changes upon Metal Coordination. Table 4 gathers the relevant bond distance, bond angle, and dihedral angle values for LPA^B, LPA^C, and their metal complexes calculated at the B3LYP/6-311++G(d,p) level in a vacuum and aqueous environment. $C_\alpha-C_7$, $C_\alpha-C_\beta$, and $C_\alpha-N$ are the three bonds considered to study the influence of metalation on the C_α-atom geometry of LPA. Out of these, the $C_\alpha-C_7$ and $C_\alpha-N$ bonds of the complexes show largest variations up to 0.026 Å in the aqueous phase and 0.045 Å in a vacuum from that of the free LPA conformers. On other hand, among the three bond angles pertaining to the C_α-atom geometry of LPA, viz. $N-C_\alpha-C_7$, $N-C_\alpha-C_7$, and $C_7-C_\alpha-C_\beta$, the latter two angles are found to deviate up to a maximum of 5.7° in the aqueous phase and 4.8° in a vacuum, respectively, as compared to those of the complexes. These variations in the bond distances and bond angles are indicative of the fact that metalation through the NH_2 and COO^- moieties of LPA can have a significant effect on the geometrical features of its C_α atom. Additionally, divergence up to 0.038 Å in the aqueous phase (0.057 Å in vacuum) reveals that the bond distances of the $C_\beta-C_1$, $C_7{=}O_b$, and C_7-O_a bonds of LPA are also markedly changed. Collected in Table 4 are gas and aqueous phase values for the five dihedral angles related to the backbone structural aspects of the two LPA conformers and their metal complexes. A largest divergence of 37.5° in the aqueous phase and 59.8° in a vacuum for the $O_a-C_7-C_\alpha-C_\beta$ dihedral in the complexes arising from LPA^B compared to those of the free LPA^B reflects that this conformer needs to go through a larger amount of intrinsic structural reorganizations compared to the LPA^C conformer to be able to interact with the metal ions via its NH_2 and COO^- moieties. Table 4 also represents the vacuum and aqueous phase bond distance values for the M−O and M−N bonds of the metal complexes along with their Wiberg bond indices[62] calculated at the B3LYP/6-311++G(d,p) and BHandHLYP/6-311++G(d,p) levels. It is apparent from these data that the BHandHLYP method performs better than the B3LYP in predicting the bond situations as well as the values of the bond indices in the metallic complexes of LPA. For example, the B3LYP level predicted bond indices for the $Ni(LPA^C)_2$ (0.337 and 0.364 for M−O and M−N bonds in aqueous phase respectively) and $Cu(LPA^C)_2$ (0.182 and 0.199 for M−O and M−N bonds in aqueous phase respectively) seem unreal in view of the Irving−Williams series.

SUMMARY AND CONCLUSIONS

Environmentally friendly synthetic procedures have been implemented to demonstrate the essentially similar metal-coordinating motifs of LPA to the dications of nickel, copper, and zinc in both aqueous and solid phases. The synthesized 1:2 (M^{+2}/LPA) complexes are characterized by means of various physicochemical and spectral techniques generating an array of information that afford us to illustrate the simultaneous involvements of the NH_2 and COO^- groups in metal-binding, geometry of the complexes around the metal cores, their optical properties, and thermal behaviors, in addition to other physical and chemical features. Electrochemical analysis confirms a +2 oxidation state for the copper ion in the $Cu(LPA)_2$ complex. The molecular structures of the metal complexes are designed involving the most stable LPA conformers as determined at the MP2/6-311++G(d,p) level. The molecular properties of the complexes, calculated using B3LYP, BHandHLYP, and dispersion-corrected B3LYP (at DFT-D2) methods in combination with the 6-311++G(d,p) basis set, are analyzed in view of their gas and aqueous phase interaction enthalpies and Gibbs energies, harmonic vibrational frequencies, UV−vis spectra, partial atomic charges, Wiberg bond indices, HOMO−LUMO energy gaps, and dipole moments. The thermodynamic parameters and NPA charges suggest a binding affinity order of $Cu^{2+} > Ni^{2+} > Zn^{2+}$, which obeys the Irving−Williams series. Cation−π interactions established by the aromatic side-chain moiety of the LPA^C conformer (λ∼ −70°) with the metal ions impart enhanced stability to the complexes. While the BHandHLYP functional performs much better than B3LYP in ascribing the thermodynamic stabilities of the complexes, the dispersion-corrected B3LYP (at DFT-D2) method outshines

dx.doi.org/10.1021/ci500500k | J. Chem. Inf. Model. XXXX, XXX, XXX−XXX

the BHandHLYP functional in reproducing the experimentally observed vibrational modes. Metalations by the dications of transition elements are found to modify the geometrical features about the C_α, C_7, and N atoms of LPA.

■ ASSOCIATED CONTENT

Supporting Information

Tables S1−S6 and Figures S1−S9. This material is available free of charge via the Internet at http://pubs.acs.org.

■ AUTHOR INFORMATION

Corresponding Author

*E-mail: guna_das78@yahoo.co.in.

Present Address

[†]Department of Chemistry, North Eastern Hill University, Shillong-793022, India

Notes

The authors declare no competing financial interest.

■ ACKNOWLEDGMENTS

The authors acknowledge the financial assistance from the Special Assistance Program of the University Grants Commission (UGC), New Delhi, India, to the Department of Chemistry, N.E.H.U. G.D. is grateful to the Council of Scientific and Industrial Research, New Delhi, India, for generous allocation of computational facilities through the Research Project No. 37(1481)/11/EMR-II. S.M. is thankful to the UGC, New Delhi, for financial assistance through a research fellowship. The authors also appreciate the analytical services provided by SAIF, N.E.H.U.

■ REFERENCES

(1) Yamauchi, O.; Odani, A.; Takani, M. Metal−amino acid chemistry. Weak interactions and related functions of side chain groups. *J. Chem. Soc., Dalton Trans.* **2002**, 3411−3421.

(2) Merola, J. S. Transition Metal Complexes of Amino Acids and Related Ligands and Their Use as Catalysts, Anti-Microbials, and Anti-Cancer Agents. U.S. Patent 0096090 A1, April 18, 2013.

(3) Dudev, T.; Lim, C. Metal-Binding Affinity and Selectivity of Nonstandard Natural Amino Acid Residues from DFT/CDM Calculations. *J. Phys. Chem. B* **2009**, *113*, 11754−11764.

(4) Rode, B. M. Peptides and the origin of life. *Peptides* **1999**, *20*, 773−786.

(5) Glusker, J. P. Structural aspects of metal liganding to functional groups in proteins. *Adv. Protein Chem.* **1991**, *42*, 1−76.

(6) Severin, K.; Bergs, R.; Beck, W. Bioorganometallic Chemistry-Transition Metal Complexes with α-Amino Acids and Peptides. *Angew. Chem., Int. Ed.* **1998**, *37*, 1634−1654.

(7) Rodgers, M. T.; Armentrout, P. B. A Thermodynamic "Vocabulary" for Metal Ion Interactions in Biological Systems. *Acc. Chem. Res.* **2004**, *37*, 989−998.

(8) Xie, J.; Liu, W.; Schultz, P. G. A Genetically Encoded Bidentate, Metal-Binding Amino Acid. *Angew. Chem., Int. Ed.* **2007**, *46*, 9239−9242.

(9) Lu, Y. Design and engineering of metalloproteins containing unnatural amino acids or non-native metal-containing cofactors. *Curr. Opin. Chem. Biol.* **2005**, *9*, 118−126.

(10) Lu, Y.; Berry, S. M.; Pfister, T. D. Engineering Novel Metalloproteins: Design of Metal-Binding Sites into Native Protein Scaffolds. *Chem. Rev.* **2001**, *101*, 3047−3080.

(11) Dudev, T.; Lim, C. Metal Binding Affinity and Selectivity in Metalloproteins: Insights from Computational Studies. *Annu. Rev. Biophy.* **2008**, *39*, 97−116.

(12) Remko, M.; Fitz, D.; Rode, B. M. Effect of metal ions (Li^+, Na^+, K^+, Mg^{+2}, Ca^{+2}, Ni^{+2}, Cu^{+2} and Zn^{+2}) and water coordination on the structure and properties of L-histidine and zwitterionic L-histidine. *Amino Acids* **2010**, *39*, 1309−1319.

(13) Fraústo da Silva, J. J. R.; Williams, R. J. P. *The Biological Chemistry of the Elements*; Oxford Univ. Press: Oxford, 1991.

(14) Bertini, I.; Sigel, A.; Sigel, H. *Handbook on Metalloproteins*; Marcel Dekker: New York, 2001.

(15) Wormald, M. R.; Petrescu, A.-J.; Pao, Y.; Glithero, A.; Elliott, T.; Dwek, R. A. Conformational Studies of Oligosaccharides and Glycopeptides: Complementarity of NMR, X-ray Crystallography, and Molecular Modelling. *Chem. Rev.* **2002**, *102*, 371−386.

(16) Ruan, C.; Rodgers, M. T. Cation-π Interactions: Structures and Energetics of Complexation of Na^+ and K^+ with the Aromatic Amino Acids, Phenylalanine, Tyrosine, and Tryptophan. *J. Am. Chem. Soc.* **2004**, *126*, 14600−14610.

(17) Rimola, A.; Sodupe, M.; Tortajata, J.; Rodríguez-Santiago, L. Gas phase reactivity of Cu^+-aromatic amino acids: An experimental and theoretical study. *Int. J. Mass Spectrom.* **2006**, *257*, 60−69.

(18) Ma, J. C.; Dougherty, D. A. The Cation-π Interaction. *Chem. Rev.* **1997**, *97*, 1303−1324.

(19) Gallivan, J. P.; Dougherty, D. A. Cation-π interactions in structural biology. *Proc. Natl. Acad. Sci. U. S. A.* **1999**, *96*, 9459−9464.

(20) Ryzhov, V.; Dunbar, R. C.; Cerda, B.; Wesdemiotis, C. Cation-π Effects in the Complexation of Na^+ and K^+ with Phe, Tyr, and Trp in the Gas Phase. *J. Am. Soc. Mass Spectrom.* **2000**, *11*, 1037−1046.

(21) Remko, M.; Fitz, D.; Broer, R.; Rode, B. M. Effect of metal Ions (Ni^{2+}, Cu^{2+} and Zn^{2+}) and water coordination on the structure of L-phenylalanine, L-tyrosine, L-tryptophan and their zwitterionic forms. *J. Mol. Model.* **2011**, *17*, 3117−3128.

(22) Siu, F. M.; Ma, N. L.; Tsang, C. W. Cation-π Interactions in Sodiated Phenylalanine Complexes: Is Phenylalanine in the Charge-Solvated or Zwitterionic Form? *J. Am. Chem. Soc.* **2001**, *123*, 3397−3398.

(23) Kaczor, A.; Reva, I. D.; Proniewicz, L. M.; Fausto, R. Importance of Entropy in the Conformational Equilibrium of Phenylalanine: A Matrix-Isolation Infrared Spectroscopy and Density Functional Theory Study. *J. Phys. Chem. A* **2006**, *110*, 2360−2370.

(24) Polfer, N. C.; Oomens, J.; Moore, D. T.; von Helden, G.; Meijer, G.; Dunbar, R. C. Infrared Spectroscopy of Phenylalanine Ag(I) and Zn(II) Complexes in the Gas Phase. *J. Am. Chem. Soc.* **2006**, *128*, 517−525.

(25) Rimola, A.; Rodriguez-Santiago, L.; Sodupe, M. Cation-π Interactions and Oxidative Effects on Cu^+ and Cu^{+2} Binding to Phe, Tyr, Trp, and His Amino Acids in the Gas Phase. Insights from First-Principles Calculations. *J. Phys. Chem. B* **2006**, *110*, 24189−24199.

(26) Larrucea, J.; Rezabal, E.; Marino, T.; Russo, N.; Ugalde, J. M. Ab Initio Study of Microsolvated Al^{+3}-Aromatic Amino Acid complexes. *J. Phys. Chem. B* **2010**, *114*, 9017−9022.

(27) Brooks, C. L., III; Karplus, M.; Pettitt, B. M. *Proteins: A Theoretical Perspective of Dynamics, Structure, and Thermodynamics*; John Wiley: New York, 1988.

(28) Garay, A. L.; Pichon, A.; James, S. L. Solvent-free synthesis of metal complexes. *Chem. Soc. Rev.* **2007**, *36*, 846−855.

(29) Mandal, S.; Das, G.; Askari, H. Interactions of *N*-acetyl-l-cysteine with metals (Ni^{2+}, Cu^{2+} and Zn^{2+}): an experimental and theoretical study. *Struct. Chem.* **2014**, *25*, 43−51.

(30) Mandal, S.; Das, G.; Askari, H. Physicochemical investigations of the metal complexes of L-valine with doubly charged ions of nickel, copper and zinc: a combined experimental and computational approach. *RSC Adv.* **2014**, *4*, 24796−24809.

(31) Miertus, S.; Scrocco, E.; Tomasi, J. Electrostatic interaction of a solute with a continuum. A direct utilization of AB initio molecular potentials for the prevision of solvent effects. *Chem. Phys.* **1981**, *55*, 117−129.

(32) Becke, A. D. Density-functional thermochemistry. III. The role of exact exchange. *J. Chem. Phys.* **1993**, *98*, 5648−5652.

(33) Lee, C.; Yang, W.; Parr, R. G. Development of the Colle−Salvetti correlation-energy formula into a functional of the electron density. *Phys. Rev. B* **1988**, *37*, 785−789.

(34) Wachters, A. J. H. Gaussian Basis Set for Molecular Wavefunctions Containing Third-Row Atoms. *J. Chem. Phys.* **1970**, *52*, 1033−1036.
(35) Hay, P. J. Gaussian basis sets for molecular calculations. The representation of 3*d* orbitals in transition-metal atoms. *J. Chem. Phys.* **1977**, *66*, 4377−4384.
(36) Note that these are the half-and-half functionals implemented in Gaussian 09 (ref 37) which are not the same as the ones proposed in: Becke, A. D. A new mixing of Hartree-Fock and local density-functional theories. *J. Chem. Phys.* **1993**, *98*, 1372−1377.
(37) Frisch, M. J.; Trucks, G. W.; Schlegel, H. B.; Scuseria, G. E.; Robb, M. A.; Cheeseman, J. R.; Scalmani, G.; Barone, V.; Mennucci, B.; Petersson, G. A.; Nakatsuji, H.; Caricato, M.; Li, X.; Hratchian, H. P.; Izmaylov, A. F.; Bloino, J.; Zheng, G.; Sonnenberg, J. L.; Hada, M.; Ehara, M.; Toyota, K.; Fukuda, R.; Hasegawa, J.; Ishida, M.; Nakajima, T.; Honda,Y.; Kitao, O.; Nakai, H.; Vreven, T.; Montgomery, J. A., Jr.; Peralta, J. E.; Ogliaro, F.; Bearpark, M.; Heyd, J. J.; Brothers, E.; Kudin, K. N.; Staroverov, V. N.; Keith, T.; Kobayashi, R.; Normand, J.; Raghavachari, K.; Rendell, A.; Burant, J. C.; Iyengar, S. S.; Tomasi, J.; Cossi, M.; Rega, N.; Millam, J. M.; Klene, M.; Knox, J. E.; Cross, J. B.; Bakken, V.; Adamo, C.; Jaramillo, J.; Gomperts, R.; Stratmann, R. E.; Yazyev, O.; Austin, A. J.; Cammi, R.; Pomelli, C.; Ochterski, J. W.; Martin, R. L.; Morokuma, K.; Zakrzewski, V. G.; Voth, G. A.; Salvador, P.; Dannenberg, J. J.; Dapprich, S.; Daniels, A. D.; Farkas, O.; Foresman, J. B.; Ortiz, J. V.; Cioslowski, J.; Fox, D. J. *Gaussian 09*, revision C.01; Gaussian, Inc.: Wallingford, CT, 2010.
(38) Andersson, M. P.; Uvdal, P. New Scale Factors for Harmonic Vibrational Frequencies Using the B3LYP Density Functional Method with the Triple-ζ Basis Set 6-311+G(d,p). *J. Phys. Chem. A* **2005**, *109*, 2937−2941.
(39) Das, G.; Mandal, S. Quantum mechanical investigations on the role of C-terminal residue in influencing the structural features of dipeptides containing N-terminal proline. *J. Mol. Graphics Modell.* **2014**, *49*, 1−10.
(40) Grimme, S. Semiempirical GGA-Type Density Functional Constructed with a Long-Range Dispersion Correction. *J. Comput. Chem.* **2006**, *27*, 1787−1799.
(41) Liu, H.; Bara, J. E.; Turner, C. H. Tuning the Adsorption Interactions of Imidazole Derivatives with Specific Metal Cations. *J. Phys. Chem. A* **2014**, *118*, 3944−3951.
(42) Reddy, A. S.; Sastry, G. N. Cation [M = H^+, Li^+, Na^+, K^+, Ca^{2+}, Mg^{2+}, NH_4^+, and NMe_4^+] Interactions with the Aromatic Motifs of Naturally Occurring Amino Acids: A Theoretical Study. *J. Phys. Chem. A* **2005**, *109*, 8893−8903.
(43) Varadwaj, P. R.; Marques, H. M. The physical chemistry of $[M(H_2O)_4(NO_3)_2]$ (M = Mn^{2+}, Co^{2+}, Ni^{2+}, Cu^{2+}, Zn^{2+}) complexes: computational studies of their structure, energetics and the topological properties of the electron density. *Theor. Chem. Acc.* **2010**, *127*, 711−725.
(44) Gould, I. R.; Cornell, W. D.; Hillier, I. H. A Quantum Mechanical Investigation of the Conformational Energetics of the Alanine and Glycine Dipeptides in the Gas Phase and in Aqueous Solution. *J. Am. Chem. Soc.* **1994**, *116*, 9250−9256.
(45) Foresman, J. B.; Frisch, A. *Exploring Chemistry with Electronic Structure Methods*, 2nd ed.; Gaussian, Inc.: Pittsburgh, PA, 1996.
(46) Freeman, F.; Le, K. T. A Computational Study of Conformations and Conformers of 1,3 Dithiane (1,3-Dithiacyclohexane). *J. Phys. Chem. A* **2003**, *107*, 2908−2918.
(47) Marques, M. A. L.; Gross, E. K. U. Time-Dependent Density Functional Theory. *Annu. Rev. Phys. Chem.* **2004**, *55*, 427−455.
(48) Geary, W. J. Use of conductivity measurements in organic solvents for the characterization of coordination compounds. *Coord. Chem. Rev.* **1971**, *7*, 81−122.
(49) Berg, J. M.; Merkle, D. L. On the Metal Ion Specificity of "Zinc Finger" Proteins. *J. Am. Chem. Soc.* **1989**, *111*, 3759−3762.
(50) Dougherty, D. A. Cation-π Interactions Involving Aromatic Amino Acids. *J. Nutr.* **2007**, *137*, 1504S−1508S (discussion 1516S-1517S).
(51) McFail-Isom, L.; Shui, X.; Williams, L. D. Divalent Cations Stabilize Unstacked Conformations of DNA and RNA by Interacting with Base Π Systems. *Biochem.* **1998**, *37*, 17105−17111.
(52) Dunbar, R. C. Complexation of Na^+ and K^+ to Aromatic Amino Acids: A Density Functional Computational Study of Cation-π Interactions. *J. Phys. Chem. A* **2000**, *104*, 8067−8074.
(53) Siu, F. M.; Ma, N. L.; Tsang, C. W. Competition between π and Non-π Cation-Binding Sites in Aromatic Amino Acids: A Theoretical Study of Alkali Metal Cation (Li^+, Na^+, K^+)-Phenylalanine Complexes. *Chem.—Eur. J.* **2004**, *10*, 1966−1976.
(54) Herlinger, A. W.; Wenhold, S. L.; Long, T. V. Infrared Spectra of Amino Acids and Their Metal Complexes. II. Geometrical Isomerism in Bis(amino acidato)copper(II) Complexes. *J. Am. Chem. Soc.* **1970**, *92*, 6474−6481.
(55) Nakamoto, K.; Morimoto, Y.; Martell, A. E. Infrared Spectra of Aqueous Solutions. I. Metal chelate compounds of amino acids. *J. Am. Chem. Soc.* **1961**, *83*, 4528−4532.
(56) Hehre, W. J.; Radom, L.; Schleyer, P. v. R.; Pople, J. A. *Ab Initio Molecular Orbital Theory*; John Wiley: New York, 1986.
(57) Lee, S. Y.; Boo, B. H. Density Functional Theory Study of Vibrational Spectra of Fluorene. *J. Phys. Chem.* **1996**, *100*, 8782−8785.
(58) Proft, F. D.; Martin, J. M. L.; Geerlings, P. On the performance of density functional methods for describing atomic populations, dipole moments and infrared intensities. *Chem. Phys. Lett.* **1996**, *250*, 393−401.
(59) Das, G.; Mandal, S. Ab initio- and density-functional studies of conformational behaviour of *N*-formylmethionine in gaseous phase. *Chem. Paper.* **2014**, *68*, 1608−1620.
(60) Lever, A. B. P. *Inorganic Electronic Spectroscopy*; Elsevier: New York, 1984.
(61) Mashaly, M. M.; Abd-Elwahab, Z. H.; Faheim, A. A. Preparation, Spectral Characterization and Antimicrobial Activities of Schiff Base Complexes Derived from 4-Aminoantipyrine. Mixed Ligand Complexes with 2-Aminopyridine, 8-Hydroxyquinoline and Oxalic Acid and Their Pyrolytical Products. *J. Chin. Chem. Soc.* **2004**, *51*, 901−915.
(62) Wiberg, K. B. Application of the pople-santry-segal CNDO method to the cyclopropylcarbinyl and cyclobutyl cation and to bicyclobutane. *Tetrahedron* **1968**, *24*, 1083−1096.